Submission to: Green Chemistry

Manuscript type: Full Article

CompassR-guided recombination unlocks design principles to stabilize a lipase in ILs with minimal experimental efforts

Haiyang Cui[1,2], Subrata Pramanik[1], Karl-Erich Jaeger[3,4], Mehdi D. Davari[1], Ulrich Schwaneberg[1,2*]*

[1]Institute of Biotechnology, RWTH Aachen University, Worringerweg 3, Aachen 52074, Germany

[2]DWI-Leibniz Institute for Interactive Materials, Forckenbeckstraße 50, Aachen 52056, Germany

[3]Institute of Molecular Enzyme Technology, Heinrich Heine University Düsseldorf, Wilhelm Johnen Strasse, Jülich, Germany

[4]Institute of Bio-and Geosciences IBG 1: Biotechnology, Forschungszentrum Jülich GmbH, Wilhelm Johnen Strasse Jülich, Germany

*Corresponding Authors: Prof. Dr. Ulrich Schwaneberg

Dr. Mehdi D. Davari

Abstract

Biocatalysis in ionic liquids (ILs) has gained enormous attention in producing biodiesel, sugar esters, and pharmaceuticals. However, hydrophilic ILs interaction with enzymes often results in reduced activity or even inactivation. In this report, we prove that intrinsic lipase stability and preservation of hydration shells of *Bacillus subtilis* lipase A (BSLA) are two synergistic design principles to retain enzymatic activity in ILs. After *in silico* screening of nine beneficial amino acid positions by the CompassR rule (in total, 172 variants), we rationally designed two variants to be constructed by site-directed mutagenesis and three libraries by site-saturation mutagenesis. With minimal experiment effort, we identified three all-around variants towards four [BMIM]-based ILs resistance. Remarkably, the variant M1a F17S/V54K/D64N/D91E/G155N had a 6.7-fold higher resistance against 40 % (v/v) [BMIM]Cl, 5.6-fold in 80 % (v/v) [BMIM]Br, 5.0-fold in 30 % (v/v) [BMIM][TfO], and 2.7-fold in 10 % (v/v) [BMIM]I compared to wild-type BSLA, respectively, while showing 1.9-fold improvement in specific activity. Computational analysis of molecular dynamics and thermodynamic stability of variants revealed the molecular basis for resistant variants M1a and M1b as synergistic enhancement of protein stability ($\Delta\Delta G_{fold}$ ranging from -4.26 to -4.80 kcal/mol) and increased hydration shell around substitutions in four ILs (up to 1.7-fold). These design principles and the gained molecular knowledge not only open the door to direct experimentalists to rationally designing promising ILs-resistant enzymes but also provide new insights into enzymatic catalysis in ILs.

Keywords: CompassR, Ionic liquid resistance, rational protein design, *Bacillus subtilis* lipase A, molecular dynamics simulation, enzyme stability

1. Introduction

Green chemistry is directed to reduce the environmental toxicity that results from the chemical compounds applied in industrial processes[1, 2]. Ionic liquids (ILs) as environmentally friendly and safer alternative solvents have gained tremendous attention for biocatalysis and biotransformations, the green and sustainable technologies, in producing pharmaceuticals [3-5], biofuels [6, 7], and other compounds [8-10]. And ILs have been employed as solvents, cosolvents, or additives in numerous enzyme and/or whole cell processes, which usually introduced improved process performance [11-16]. Biocatalysis in ILs has been extensively studied [17-20] and found that widely divergent enzymes are catalytically active in IL or aqueous biphasic IL systems [21, 22]. Russell et al. in 2000 presented the first report of enzymatic catalysis in an IL that the thermolysin-catalyzed synthesis of Z-aspartame in 1-butyl-3-methylimidazolium hexafluorophosphate (BP6) and observed competitive initial reaction rates and high enzymatic stability [17]. There is a considerable amount of reports on notable increases in enzyme stabilities in ILs containing noncoordinating anions [23, 24], and in some cases the improved (enantio)selectivities were observed [24, 25], even at high temperature like *Geobacillus thermocatenolatus* lipase [26]. Importantly, the lipase-catalyzed reactions in ILs, considering as being "green", provide more technological advantages than chemical methods due to the easy recovery of product, the high recyclability, and mild reaction conditions [10, 27-29]. Besides, lipase in ILs showed promising stability, selectivity, and production yields in biodiesel production, esterification, and other established applications [28, 30]. However, some other results suggest that the vast majority of enzymes, including lipases, often show worse resistance with reduced or no catalytic activity in hydrophilic ILs containing coordinating anions, such as nitrate, sulfate and chloride [21, 31-36]. Obviously, this limits the expansion of the application scope of biocatalysis in ILs.

Various methods to enhance the stability of enzymes in ILs have been investigated, such as chemical and charge modification [37-39], immobilization [40-43], and chemical cross-linking [36, 44]. Protein engineering by directed evolution [45, 46], and/or (semi-)rational design [36, 47-49] has proven highly useful methods to tailor enzyme properties to cost-effective production conditions. Recently, protein engineering strategies have been reported to combine both approaches and minimize experimental efforts [50], such as KnowVolution [51], MORPHING [52], ProSAR [53]. CompassR (Computer-assisted Recombination) proved that intrinsic stability, evaluated by the relative free energy of folding ($\Delta\Delta G_{fold}$), is an essential factor to gradually improve enzyme performance through efficiently recombining beneficial positions [54-56]. In our previous study, the CompassR rule (especially referring substitutions in category A with $\Delta\Delta G_{fold} < 0.36$ kcal/mol) was successfully developed to overcome the general recombination challenge that poorly performing and/or inactive variants are often obtained after recombination of 3 to 4 beneficial substitutions [54]. CompassR holds the promise to efficiently and gradually improve enzyme properties through recombination of beneficial positions that contribute to intrinsic stability, thus resulting in enzymes active in IL solutions. It has now been shown that CompassR yielded one *Bacillus subtilis* lipase A (BSLA) variant F17S/V54K/D64N/D91E, which having a 2.7-fold enhanced specific activity in 18.3 % (v/v) 1-butyl-3-methylimidazolium chloride ([BMIM]Cl) [54]. However, further improvement needs to be carried out to reveal more extensive "power" of CompassR and accelerate the application of versatile enzyme lipase in various kinds of biocatalyzed reactions.

Protein engineering of cellulase [57, 58], laccase [32-34], lipases [31, 35, 36], and others toward ILs resistance has been reported [59]. For instance, Pottkamper *et al.* isolated cellulase variants of CelA10 in a directed evolution experiment employing SeSaM technology, which showed a 5-fold higher activity compared to the wild-type (WT) in 30 % (v/v) 1-butyl-1-methylpyrrolidinium

trifluoromethane sulfonate ([BMPL][OTF]) [58]. Liu *et al.* reported that the laccase variant lcc2-M3 (F265S/A318V) displayed about 4.5-fold higher catalytic activity than the WT in 15% (v/v) 1-ethyl-3-methylimidazolium ethylsulfate ([EMIM][$EtSO_4$]) [32] after two rounds of directed evolution. *Candida antarctica* lipase B (CALB) dissolved in ILs showed reduced activity even irreversibly deactivated in ILs [44, 60-63]. In addition, BSLA is the most thoroughly studied enzyme in ILs by protein engineering [31, 35, 36, 64]. A site saturation library was experimentally constructed with the single amino acid exchanges at each position of BSLA (named as BSLA-SSM library, 181 positions; 3439 variants), and analyzed for resistance towards four ILs (e.g., [BMIM]Cl, [BMIM]Br, [BMIM]I, and [BMIM][TfO]) [64]. This study revealed that 6 - 13 % of substitutions, locating at 50 - 69 % of all amino acid positions, can improve ILs resistance. Here, we tried to meet the challenges of how all these beneficial positions can be recombined to maximize the resistance of BSLA in IL with minimal experimental efforts.

Molecular dynamics (MD) simulations and FT-IR [44, 65], CD [65, 66], DSC [67, 68], and NMR [36] of improved enzyme variant in ILs suggest the following reasons for reduced enzymatic activity and/or deactivated enzymes in ILs: (a) conformational changes resulting in diminished structural stability [35, 44, 60, 69]; (b) decreased ion-protein interactions, particularly the anion effect is dominant [35, 69, 70]; (c) competitive inhibition [69, 71]; and (d) loss of bound water [35, 60]. However, the structure-function relationship of enzymes in ILs remains elusive, and inactivation in ILs is often the result of several factors. Additional understanding of the enzymes' inactivation process and the underline mechanism in ILs is favorable for efficiently enhancing enzymes' stability in aqueous IL media. Among several technologies, MD simulations provide a complementary method to study the connection between protein dynamics and the stability of the enzyme in ILs, which has been validated to be in line with various experimental measurements [60, 69, 72].

Herein, we demonstrate that two synergic design principles (enhancing intrinsic stability and keeping the hydration shell) enable efficient catalysis of BSLA in the ILs [BMIM]Cl, [BMIM]Br, [BMIM]I, and [BMIM][TfO]. The objectives of the current work focus on (i) combining the CompassR analysis and rational selection of the positions to yield several recombinants with high enhanced multiple ILs resistance while also maintaining or increasing its activity (a current and massive challenge in the protein engineering field); (ii) gaining a molecular understanding of BSLA-IL interaction in the enzymes inactivation process to benefit rationally designing better IL resistant enzymes. These goals can be achieved through a combination of CompassR-guided recombination approach and MD simulation in four [BMIM]-based ILs with minimal experimental efforts (in total ~272 clones were screened, which were derived from two site-directed mutagenesis (SDM) variants and three site-saturation mutagenesis (SSM) libraries).

2. Methods

2.1 Recombinants generated by site-directed mutagenesis and site-saturation mutagenesis

BSLA variants were stepwise constructed by PCR according to the QuikChange site directed mutagenesis method (SDM) [39] using the primers listed in **Table S1** in SI. Site-saturation mutagenesis (SSM) libraries for the BSLA were generated with degenerate primers (NNS; N=A/T/G/C, S=C/G, encoding all 20 amino acids with 32 distinct codons; **Tables S1**) by a modified QuikChange PCR protocol [39] as in our previous studies [64, 73].

2.2 Activity assay in 96-well Microtiter Plate

Microtiter plate (MTP)-based *p*-nitrophenyl butyrate (*p*NPB) assay with culture supernatant or purified BSLA was performed as described previously [31, 64, 73]. BSLA fused to the PelB signal sequence is secreted into the culture supernatant upon expression from vector pET22b (+) in *E.*

coli BL21-Gold (DE3) [64, 73, 74]. The *p*NPB was used as the substrate to detect the activity of BSLA in the presence/absence of ILs. Lipase BSLA converts *p*NPB to *p*-nitrophenol within the hydrolysis reaction. A more detailed *p*NPB assay process was described in **section 2.3**. Variants are identified by the following three categories [75]: beneficial substitutions with improved resistance ($R_V \geq R_{WT} + 3\sigma$); unchanged substitutions with unchanged resistance ($R_V < R_{WT} + 3\sigma$ and $R_V > R_{WT} - 3\sigma$); decreased substitutions with decreased resistance ($R_V \leq R_{WT} - 3\sigma$). Residual activity is abbreviated as R, activity as A, variant as V, wild type as WT, empty vector as EV, standard deviation as σ. Residual activities of WT/variants were calculated as the following equation 1:

$$\text{Residual activity } (R_{WT/V}, \%) = \frac{slope(WT/\text{variant}-Ev)\ IL\ cosolvent}{slope(WT/\text{variant}-E\ )\ buffer} \quad (1)$$

The normalized activity was calculated according to the quantity of cells measured by OD_{600}. One unit (U) of enzyme activity was defined as the amount of enzyme releasing 1.0 mmol of *p*-nitrophenol per minute under the assay conditions [31]. All data shown are average values from measurements in triplicates or more.

2.3 Screening of SSM libraries in the presence of ILs

The screening assay with 18.3 % (v/v) [BMIM]Cl was performed in flat-bottomed, polystyrene 96-well MTPs (Greiner Bio-One). This [BMIM]Cl concentration for "BSLA-SSM" library screening was chosen to ensure a R_{WT} of ~30%, a suitable condition to estimate the performance change of the BSLA variant. In each well, the culture supernatant (10 µL) was incubated with [BMIM]Cl solution (90 µL; 18.3 µL [BMIM]Cl + 71.7 µL TEA buffer) or with TEA buffer (90 µL, 50 mM, pH 7.4) for 2 h at room temperature (RT) on a microtiter shaker (800 rpm; Edmund Bühler, Hechingen, Germany). Freshly prepared 100 µL substrate solution (0.5mM *p*NPB final concentration, 90 % (v/v) TEA buffer and 10 % (v/v) acetonitrile) was added, and A_{410} values were

measured at RT over 8 min on an Infinite M200 Pro microtiter plate reader (Tecan, Maennedorf, Switzerland). The function of organic solvent acetonitrile was dissolving the substrate *p*NPB. All the identified variants were rescreened, at least in triplicate, to identify the improved variants. The same procedure was also performed for four [BMIM]-based ILs at various concentrations with purified BSLA variants. IL resistance of BSLA (WT or variant) was evaluated as activity in the presence of IL divided by activity in the absence of IL [31, 64]. In other words, IL resistance was normalized by the R_{WT} and shown in equation 2:

$$\text{IL resistance relative to WT} = \frac{R_V \; in \; IL}{R_{WT} \; in \; IL} \quad (2)$$

2.4 Growth of bacteria in flask and purification of BSLA

E. coli BL21-Gold (DE3) harboring pET22-*bsla* was grown in Erlenmeyer flasks. BSLA variants were purified as previously described by Cui *et al.* [75]. In detail, the main expression culture with the medium was cultivated at 30 °C (250 rpm) for 16 h. Cells were harvested by centrifugation (4,000 × g, 15 minutes) and then resuspended in lysis buffer (25 mM Tris-Cl, pH 7.5, 150 mM NaCl, 10 mM imidazole, and 0.5 mg/mL lysozyme). Cells were disrupted by sonication and debris removed by centrifugation (15,000 × g, 1 h) to get the supernatant. The obtained supernatant was then applied to the Protino1 Ni-TED 2000 packed columns from Macherey-Nagel. After, the salts were removed by a PD-10 desalting column from GE Healthcare (Germany). The purified lipases were stored at storage buffer (10 mM glycine, pH 10.5) in small aliquots at -80 °C. The purity of BSLA variants was analyzed by SDS-PAGE (5 % stacking gel and 12 % separating gel) in **Figure S1**.

2.5 Stability analysis of BSLA variants

The structure of BSLA variants and their relative free energy of folding energies ($\Delta\Delta G_{fold} = \Delta G_{fold,sub} - \Delta G_{fold,wt}$) were computed using FoldX 4 [76] implemented in YASARA plugin [77] in YASARA v17.4.17 [78, 79] as previously reported [54]. The structure coordinate of wild-type BSLA was retrieved from the Protein Data Bank (PDB ID: 1i6w [80] Chain A, resolution 1.5 Å) as the initial structure for FoldX analysis. Rotamer and energy optimizations were performed using the "RepairObject" command to correct the residues that have non-standard torsion angles. "Mutate residue" and "Mutate multiple residues" command were applied to calculate the $\Delta\Delta G_{fold}$ of single substitutions and recombinants, respectively. We used default for temperature (298 K), ionic strength (0.05 M), and pH (7). The $\Delta\Delta G_{fold}$ calculation was performed five times and averaged for each substitution.

2.6. Molecular dynamics simulations

MD simulations of BSLA WT and variants were performed in consistent with experimental condition 40 % (v/v) [BMIM]Cl, 10 % (v/v) [BMIM]I, 80 % (v/v) [BMIM]Br, and 30 % (v/v) [BMIM][TfO] using the GROMACS v5.1.2 package [81-84] with GROMOS96 54a7 force field as previous reports [85-88]. All IL models were taken from our previous work employing GROMOS96 54a7 force field [88], which reproduced the properties of the water/IL mixture in perfect agreement with the experimental data [69]. GROMOS96 54a7 force field is applied for MD simulations. Protonation states were assigned based on pKa calculation using PROPKA method [89] and employing the PDB2PQR server [90]. The protonation state of the catalytic triad was considered based on the catalytic mechanism of lipase. Particularly, the protonation state was assigned to $N_{\delta 1}$ atom of catalytic residue H156 based on the proton transfer mechanism involved in the activation of the hydroxyl group of the catalytic serine of the catalytic triad [91-93]. Hydrogens were added to the protein molecule by using the pdb2gmx tool in GROMACS. The protein molecules were

placed in a cubic simulation box (10 Å from the box edge). $BMIM^+$ cations were inserted into simulation box according to concentration of [BMIM]Cl (40 % v/v), [BMIM]I (10 % v/v), [BMIM]Br (80 % v/v), and [BMIM][TfO] (30 % v/v) in each system, respectively. The system was solvated with the SPC/E water model [94, 95]. To neutralize the system, Cl^-, Br^-, I^-, and TfO^- were added into the simulation box for[BMIM]Cl, [BMIM]Br, [BMIM]I, and [BMIM][TfO] cosolvents, respectively as previously reported [69]. For system ionization, electrostatic interactions were calculated by applying the Particle Mesh Ewald (PME) method [96, 97]. Short-range electrostatic interactions and van der Waals (vdW) interactions were calculated using a cutoff value of 1.0, respectively. Energy minimization of the whole system for each IL was performed individually using the steepest descent minimization algorithm until the maximum force reached 1000.0 kJ mol^{-1} nm^{-1}. Subsequently, system equilibration was performed under NVT and NPT ensemble. In NVT (canonical ensemble), the amount of substance (N), volume (V), and temperature (T) are conserved. In NPT (isothermal-isobaric ensemble), the amount of substance (N), pressure (P), and temperature (T) are conserved. The NVT equilibration was conducted at a constant temperature of 300 K for 100 ps with a time step of 2 fs. Initial random velocities were assigned to the atoms of the molecules according to the Maxwell–Boltzmann algorithm at the same temperature. The NPT equilibration was conducted at a constant temperature of 300 K for 100 ps with a time step of 2 fs, respectively. The Berendsen thermostat [98] and Parrinello-Rahman pressure [99] coupling was used to keep the system at 300 K, the time constant (τT) of 0.1 ps, and 1 bar pressure, the time constant (τP) of 2 ps. The production run was carried out in triplicate using NPT ensemble for 100 ns with a time step of 2 fs at a constant temperature of 300 K. LINCS algorithm was implemented to constrain all bonds between hydrogen and heavy atoms. Simulation trajectories were visualized and analyzed using VMD 1.9.1 [100] and GROMACS tools [81-84].

3. Results and Discussion

The result section is divided into four parts. The first part describes the workflow of the CompassR-guided recombination approach (**Figure 1**). In detail, Step 1-3 shows how to select substitutions that can be beneficially recombined regarding the CompassR rule. In total, 172 BSLA substitutions on nine beneficial positions were analyzed. In Step 4-5, concerning the diversity of identified substitutions, two SDM variants and three SSM libraries were rationally designed. In the second part, the improved [BMIM]Cl resistant variants were obtained with minimal screening effort (~272 variants). In the third part, multi-ILs resistance and activity profiles of five purified variants were investigated at varying concentrations of four ILs (i.e., [BMIM]Cl, [BMIM]Br, [BMIM]I, [BMIM][TfO]). In the last two parts, through stability analysis and MD simulation studies of two highly enhanced variants in four ILs, we discovered two design principles governing the highly multi-ILs resistant BSLA variants.

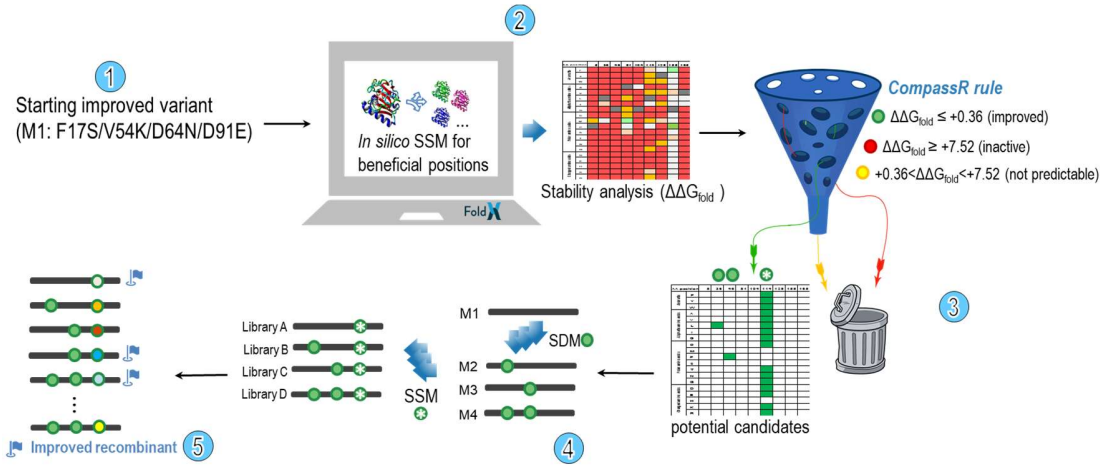

Figure 1. CompassR-guided recombination approach to improve BSLA resistance in [BMIM]Cl. ○,1 The improved starting variant can be obtained from directed evolution or rational design campaign; ○,2 *In silico* site saturation mutagenesis on beneficial amino acid positions to generate the stability ($\Delta\Delta G_{fold}$) landscape; ○,3 Identification of potential candidates by CompassR rule (category A: $\Delta\Delta G_{fold} < +0.36$ which can be predictably beneficially recombined, B: $+0.36 < \Delta\Delta G_{fold} < +7.52$ which showed unpredictable recombinants; C: $\Delta\Delta G_{fold} > +7.52$ which yield inactive recombinants); ○,4 Two step recombination process with SDM and SSM method was

applied for recombination concerning the positional diversity of candidates; ○,5 Highly improved recombinant enzyme with targeted property is obtained (e.g., IL resistance).

3.1 CompassR-guided recombination to improve BSLA resistance in [BMIM]Cl

The following five steps were taken in the CompassR-guided recombination approach (**Figure 1**):

Step1: The improved starting variant was obtained from directed evolution and/or rational design. The BSLA variant M1 F17S/V54K/D64N/D91E was chosen as the starting point, which was obtained from our previous CompassR study [54] with distinct stability and 2.7-fold improvement towards [BMIM]Cl resistance (**Figure 2a**).

Step2: *In silico* site saturation mutagenesis on beneficial amino acid positions to generate the stability landscape. Nine beneficial positions towards [BMIM]Cl resistance, identified previously [54] but not well explored yet, were selected for recombination with BSLA M1 to improve IL resistance further. The stability landscape of 172 variants on nine positions is evaluated by $\Delta\Delta G_{fold}$ in kcal/mol (172 = 19 × 9 + wild-type, **Figure 2b**). The vast majority were destabilizing ($\Delta\Delta G_{fold} > 0$), except the substitutions on position G155. The latter indicates many positions might tolerate only minimal sequence variation, especially P5, G46, and G10. Corresponding results were also confirmed by evolutionary conservation analysis (**Table S2**). In terms of the IL resistance pattern of 172 substitutions in the BSLA-SSM library [54, 64], thirty-eight variants (green block in **Figure 2c**) had improved [BMIM]Cl resistance. The latter variants meet the pre-requirement of the CompassR rule that the variant must be beneficial [64].

Step 3: Identification of potential candidates by CompassR rule. Figure 2d-e shows the results of comparing the [BMIM]Cl resistance and stability performance. The criteria of selecting the potential candidates are as follows: (i) the properties of an enzyme (e.g., [BMIM]Cl resistance

in the current study) show improvement ($R_V \geq R_{WT} + 3\sigma$) ; (ii) the $\Delta\Delta G_{fold}$ value of substitution should be lower than +0.36 kcal/mol, belonging to the category A in CompassR rule. Regarding the above criteria, two beneficial substitutions (A81M and V165L) and one beneficial position (position 155), which were located in the region I ($\Delta\Delta G_{fold} \leq +0.36$ kcal/mol) with predictable recombination behavior, were finally selected for further recombination. Besides, the remaining beneficial BSLA substitutions were mostly located in regions II and III with unpredictable or inactive recombination behavior.

Step 4-5: Two-step experimental recombination process to yield highly improved recombinants. According to the distribution characteristics of the identified substitutions in Step 3, we designed the following two-step recombination process to yield the enhanced variants. Firstly, the SDM method was directly applied to introduce A81M and V165L into BSLA M1, respectively. This led to the generation of recombinants M2 (F17S/V54K/D64N/D91E/A81M) and M3 (F17S/V54K/D64N/D91E/V165L), respectively. In the next step, position G155 of the parent variants M1, M2, and M3 were subjected to SSM to explore the full natural diversity, respectively.

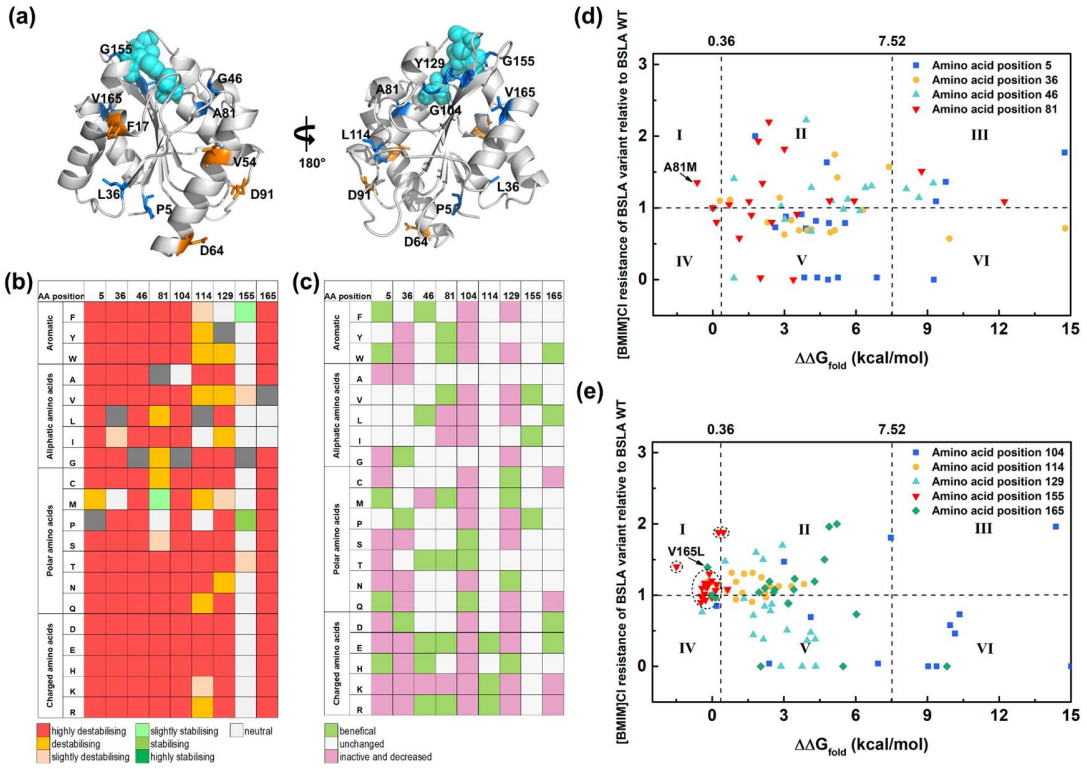

Figure 2. Performance of BSLA single substitutions. (**a**) Visualization of the thirteen beneficial amino acid positions in the 3D structure of the BSLA wild type (PDB: 1i6w [80], Chain A) using Pymol [2]. Amino acid positions of the starting variant M1 (F17S/V54K/D64N/D91E) are presented as orange sticks. The nine selected beneficial amino acid positions are presented as blue sticks. The catalytic triad residues (S77, D133, H156) are presented as cyan spheres. (**b**) Stability landscape of nine amino acid positions. $\Delta\Delta G_{fold}$ of single substitutions (in kcal/mol) are calculated by FoldX [76] and regarded as highly stabilizing (< −1.84), stabilizing (−1.84 to −0.92), slightly stabilizing (−0.92 to −0.46), neutral (−0.46 to +0.46), slightly destabilizing (+0.46 to +0.92), destabilizing (+0.92 to +1.84), and highly destabilizing (> +1.84). (**c**) [BMIM]Cl resistance pattern on nine amino acid positions (P5, L36, G46, A81, G104, L114, Y129, G155, and V165). Correlation between stability ($\Delta\Delta G_{fold}$) and ionic liquid [BMIM]Cl resistance of BSLA single substitutions on amino acid position (**d**) P5, L36, G46, A81 and (**e**) position G104, L114, Y129, G155, V165. The ionic liquid resistance was measured at 18.3 % (v/v) [BMIM]Cl. Six regions I to VI were identified by applying the CompassR rule for beneficial and non-beneficial variants. Regarding the CompassR rule[54], the arrow and short dash circle map the promising substitution(s) and position(s) for recombination, respectively.

3.2 Screening for highly improved BSLA recombinants towards [BMIM]Cl resistance

In the SDM recombination process, both recombinant BSLA M2 and M3 showed 7.5-fold and 9-fold [BMIM]Cl resistance improvements when compared to BSLA WT, respectively (**Figure 3** and **Table S3**). To achieve a 95% probability of substitutions coverage regarding randomization at one amino acid position, ~90 clones in each SSM library were screened (oversampling) [101]. The active ratio of recombinants was between 37.0 - 77.8% in the SSM libraries A, B, and C (**Table S3**). The high active proportion of recombinants in both SDM and SSM recombination stages agrees well with the previously reported CompassR studies [54]. After screening ~90 clones in library A, three variants with further increased [BMIM]Cl resistance were identified (i.e., M1a: 4.9-fold, M1b: 4.3-fold, M1c: 4.1-fold, **Figure 3**). However, libraries B and C do not yield further improved variants. **Table S3** contains the normalized activity in the buffer of five identified BSLA variants and shows up to 3.5-fold improvement (e.g., M1c) compared to BSLA WT. These results further confirm the CompassR rule that when substitutions located in category A ($\Delta\Delta G_{fold} \leq +0.36$ kcal/mol) are recombined, one can expect active and property improved recombinants [54]. As shown in **Table S4**, the CompassR-guided recombination approach has a higher ratio to yield the active variants and obtain the improved variant but less screening effort than other reported (semi-)ration design approach [102-106]. These results indicate that the current approach has a better success rate on improving the enzymatic properties with reduced laborious experiments.

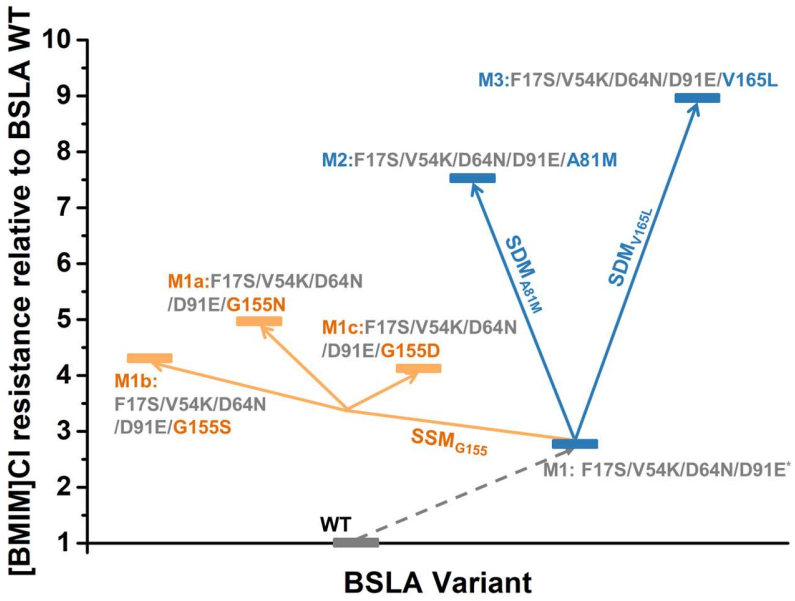

Figure 3. The resistance of the identified BSLA variants in [BMIM]Cl relative to BSLA WT in a two-step recombination procedure. The applied recombination method of variants obtained by SDM and SSM is shown with blue and orange arrow lines, respectively. BSLA variant M1 (F17S/V54K/D64N/D91E, marked with an asterisk), as the starting point in this study, was obtained from previous work [54]. Only IL variants with improved resistance from the SSM library are shown and compared to BSLA WT. The concentration of [BMIM]Cl is 18 % (v/v). All data shown are average values from measurements in triplicates or more.

3.3 Multiple ionic liquid resistance profiles of the improved BSLA recombinants

ILs resistance profiles of the five purified BSLA recombinants (i.e., M1a, M1b, M1c, M2, and M3) and BSLA WT were investigated at various [BMIM]Cl, [BMIM]I, [BMIM]Br, and [BMIM][TfO] concentrations. For all BSLA recombinants, these profiles were shifted to higher residual activities over nearly the entire range of investigated [BMIM]Cl concentration (**Figure 4**). These results suggested that the improvements were not limited to the [BMIM]Cl concentration employed. The "best" performance of recombinants occurred in 40 % (v/v) [BMIM]Cl, showing that BSLA M1a, M1c, and M2 had almost 6.7-fold, 6.3-fold, and 4.2-fold higher IL resistance when compared to BSLA WT, respectively. Regarding the remaining three ILs (i.e., [BMIM]I,

[BMIM]Br, and [BMIM][TfO]), ILs resistance profiles of most recombinants were shifted toward high IL concentration as well (**Figure 4b-c**). Few recombinants, e.g., M1a and M1c, presented greater residual activities at low ILs concentrations than WT, suggesting that the enzyme activity was highly dependent on IL concentration and introduced substitutions. Similar profiles were also observed in other lipase-IL systems, e.g., *Pseudomonas* sp. lipase in imidazolium-based ILs [107], Lip1 from thermophilic bacterium ID17 in [BMIM][PF6] and [BMIM][BF4] [108], and *Aspergillus niger* lipase in cholinium-based ILs [109]. They might result from that small amount of IL molecules perfectly interact with the enzyme, inducing conformational changes and making the enzyme more functional for catalytic activity. Unexpectedly, the purified M2 and M3 had worse IL resistance profiles than WT in ILs while showing the excellent [BMIM]Cl resistance for their crude supernatant. The possible reason could be that additional protein or hydrophobic compounds in the crude supernatant somehow "save" the enzyme from the IL's attack. Notably, BSLA M1a had almost 5.6-fold higher resistance in 80 % [BMIM]Br, 5.0-fold in 30 % (v/v) [BMIM][TfO], 2.7-fold in 10 % [BMIM]I. Similarly, BSLA M1c showed 4.8-fold higher resistance in 80 % (v/v) [BMIM]Br, 3.8-fold in 15 % (v/v) [BMIM][TfO], 2.5-fold in 10 % (v/v) [BMIM]I. These results suggested that BSLA variants generated by CompassR-guided recombination, especially M1a and M1c, have promising multi-ILs resistance characters.

In addition, the purified variant M1a, M1b, and M1c were studied more closely by investigating the specific activity at 40 %(v/v) [BMIM]Cl, 10 %(v/v) [BMIM]I, 80 %(v/v) [BMIM]Br, and 30 %(v/v) [BMIM][TfO] (**Figure S2**). All three variants, especially M1a and M1b, showed noticeably improved specific activity in both buffer (1.9-2.2 fold) and [BMIM]-halogen ILs (1.1-fold to 2.5-fold), and more details are described in SI. Summarily, through investigating four ILs resistance and specific activity profiles, we obtained three all-around BSLA recombinants (especially M1a

and M1b) with significantly increased multiple biochemical characteristics (i.e., four ILs resistance and specific activity), simultaneously.

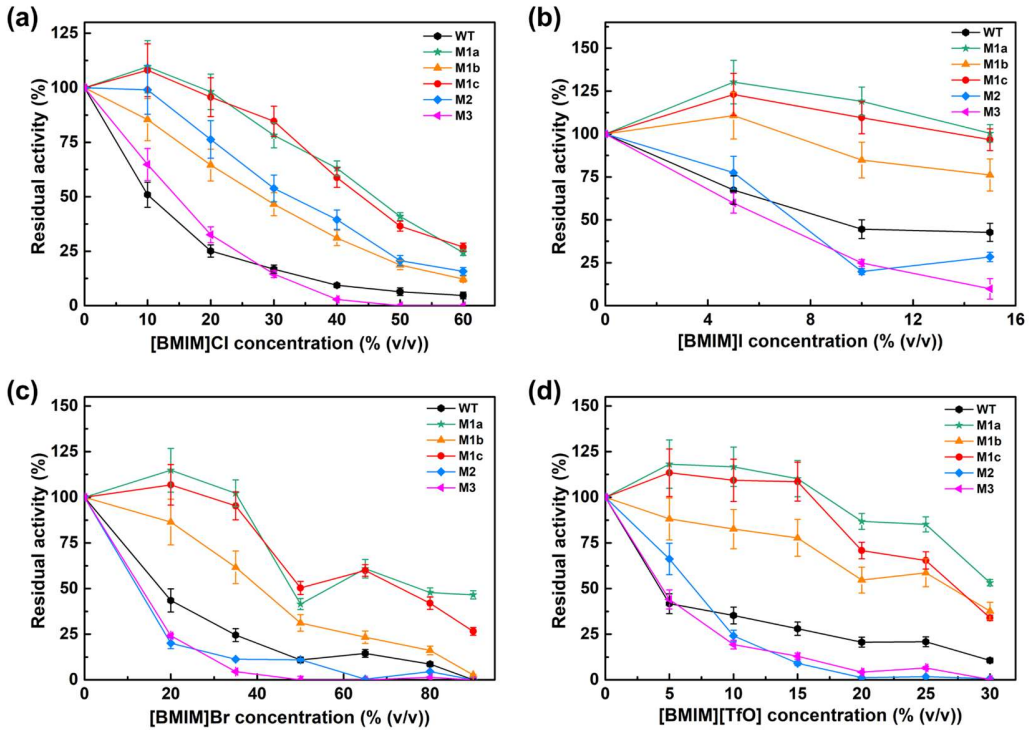

Figure 4. Resistance relative to WT of purified selected BSLA recombinants in varied concentration of (**a**) [BMIM]Cl, (**b**) [BMIM]I, (**c**) [BMIM]Br, and (**d**) [BMIM][TfO]. Resistance was measured after incubating for 2h in ILs at room temperature. M1a: F17S/V54K/D64N/D91E/G155N; M1b: F17S/V54K/D64N/D91E/G155S; M1c: F17S/V54K/D64N/D91E/G155D; M2: F17S/V54K/D64N/D91E/A81M; M3: F17S/V54K/D64N/D91E/V165L. All data shown are average values from measurements in triplicates or more.

3.4 Design principle 1: intrinsic enzyme stability

CompassR employs $\Delta\Delta G_{fold}$ (intrinsic enzyme stability) as the predominant factor to ensure that enzymes are active after several iterative recombinations. As shown in **Table 1**, for all the recombinants, the difference between sum $\Delta\Delta G_{fold}$ of substitutions and overall $\Delta\Delta G_{fold}$ of recombinant is much higher than 0.46 kcal/mol (the standard deviation of FoldX), indicating

synergetic effects among each substitution. Also, M1a, M1b, and M1c had a highly stabilizing structure with $\Delta\Delta G_{fold}$ ranging from -4.19 to -4.80 kcal/mol. Generally, enzymes must achieve a stable fold to function correctly [54]. And the variants that have higher stability tend to have higher protein fitness [110]. Intrinsic stability is a feature that inherent to the protein itself. In our BSLA experiments, the CompassR recombination results suggested that intrinsic stabilization (decreased $\Delta\Delta G_{fold}$) and enzymatic activity are not conflicting and can jointly be enhanced by recombination as shown in the stepwise increased resistance against the ILs. Besides, the intrinsic stabilization is most likely to be an independent factor to guide the better enzyme design, which is not related to the external environment, such as the different structure of ILs. Generally, enzymes must achieve a stable fold to function correctly [54], and the variants that have higher stability tend to have higher protein fitness [110]. Consequently, this finding proved that the intrinsic stabilization of recombinants is favorable to the IL resistance properties of BSLA and most likely represents a general design principle to improve other properties of other enzymes. Interestingly, the BSLA stability in Br- and Cl-based ILs can be affected at a broader range of concentration than the BSLA in I- and Tfo-based ILs (**Figure 4**). Indeed, beside the advanced intrinsic stabilization, other factors might also play critical roles in governing the ILs resistance of enzymes (see **section 3.5**).

Table 1. Stability analysis of BSLA recombinants

Variant	Substitutions[a]	Sum $\Delta\Delta G_{fold}$ of substitutions (kcal/mol) [a,d]	Overall $\Delta\Delta G_{fold}$ of recombinants (kcal/mol) [b,d]
M1	F17S/V54K/D64N/D91E[54]	+0.52	+0.99
M1a	F17S/V54K/D64N/D91E/G155N	+0.69	-4.26
M1b	F17S/V54K/D64N/D91E/G155S	+0.06	-4.80
M1c	F17S/V54K/D64N/D91E/G155D	+0.70	-4.19
M2	F17S/V54K/D64N/D91E/A81M	-0.13	+0.60

M3	F17S/V54K/D64N/D91E/<u>V165L</u>	+0.33	-0.80

[a] To compare to the starting variant M1 from previous work [54], the new recombined substitution(s) were marked with an underline.

[b] "Mutate residue" command was applied to calculate the $\Delta\Delta G_{fold}$ of every single substitution. Sum $\Delta\Delta G_{fold} = \Delta\Delta G_{fold,sub1} + \Delta\Delta G_{fold,sub2} + \Delta\Delta G_{fold,sub3} + \cdot + \Delta\Delta G_{fold,subX}$

[c] "Mutate multiple residues" command was applied to calculate the overall $\Delta\Delta G_{fold}$ of recombinants.

[d] Due to the accuracy of the FoldX method in prediction of relative folding free energies is reported to be 0.46 kcal/mol, and we defined that the synergistic effect occurs when $|\text{Sum } \Delta\Delta G_{fold} - \text{Overall } \Delta\Delta G_{fold}| > 0.46$ kcal/mol. The $\Delta\Delta G_{fold}$ calculations were performed five times and averaged for each variant.

3.5 Design principle 2: keeping hydration shells of enzyme

The interaction between the BSLA variant (M1a, M1b) and water/four ILs was simulated throughout three independent 100 ns MD runs. BSLA WT was also involved for better comparison under different IL. The selection of the specific ILs concentrations for MD simulation is regarding the condition that performs the "best" ILs resistances towards BSLA M1a and M1b. Structural properties (i.e., RMSD, RMSF, R_g, and SASA) and the solvation phenomenon (i.e., water, $BMIM^+$, and anion) were analyzed. The results of RMSD and R_g demonstrate that the structures of BSLA variants remain stable comparing to BSLA WT in water and all four ILs (i.e., [BMIM]Cl (40 % v/v), [BMIM]I (10 % v/v), [BMIM]Br (80 % v/v), and [BMIM][TfO] (30 % v/v) (see more details in SI, **Figure S3-S5**). Therefore, conformational changes in BSLA variants are consistent with the thermodynamic stability analysis results in **Section 3.4**.

Also, we determined the solvation effect from substitutions (polar and charged residue) on improving the resistance and activity of BSLA in ILs. The spatial distribution function (SDF) in **Figure 5a** and **S6** show the distribution of water and ILs molecules at the BSLA surface. In general, water molecules are stripped off by the ILs molecules (**Figure 5a-b**). The IL molecules

interact with the protein surface, causing a heterogeneous distribution of ILs at the BSLA surface. Surprisingly, although the ILs concentrations varied from 10 to 80% (v/v), the number of water molecules was significantly enhanced on the surface of both variants compared with BSLA WT (**Figures 5b**). In terms of substitution site, it was found that all substitutions attract a surprisingly enhanced number of water molecules (**Figures 5c,** up to 1.7-fold improvement) in water and ILs systems. These results demonstrated that the substituted site is the source of global hydration change. Besides, it is observed that the retention of water molecules is varied based on concentrations of ILs. For instance, a relatively lower number of surface water molecules were retained in [BMIM]Br due to its higher concentration (80 % v/v) compared with other ILs. In general, we can see that variant M1a F17S/V54K/D64N/D91E/G155N retains a higher number of water molecules compared to M1b F17S/V54K/D64N/D91E/G155S. In this regard, Asn manifests higher a potency to recover essential water molecules on the surface than Ser residue. The latter agrees well with the notion that the more hydrophilic Asn (hydropathy index -4.5) retained higher water molecules over the less hydrophilic Ser residue (hydropathy index -0.8) [111]. Generally, enzyme hydration is a fundamental aspect in non-aqueous enzymology since water molecules determine to a great extent the structural and dynamic properties of the enzyme [55, 69, 75, 112]. These observations also confirmed our previous hypothesis that that surface hydration of BSLA is essential for modifying the stability of BSLA in non-conventional media [69, 75, 113].

Considering the dominant effect of cations and/or anions, we performed a quantitative analysis of the number of cations (**Figure 5c** and **5e)** and anions (**Figure S7** in SI) in the first solvation shell of BSLA WT and variants. The main results showed that $BMIM^+$ cations interact predominantly in the case of halogenated-[BMIM]. WT and both variants M1a and M1c remain similar $BMIM^+$ amount in [BMIM]Cl, [BMIM]Br, and [BMIM]I (**Figure 5c**, see detailed

description in SI). Consistent with previous experimental findings [114], $BMIM^+$ cation interacted to surface residues via hydrophobic and cation-π interaction obtained from the crystallographic investigation. Moreover, anions remained mostly in the bulk of water (**Figure S5**). However, $BMIM^+$ and TfO^- interact with almost equal potency with BSLA WT and variants (**Figures 5a, 5c,** and **S7**, see more detailed description in SI). All these results demonstrated that IL molecules influence the enzymatic reactions by different destabilization mechanisms because the combinations of cations and anions alter the physicochemical properties of ILs [69, 115-117]. In addition, there is no universal or predominant trend in terms of the structural change and solvation phenomenon in the active site (**Figure S4** and **S8**, see detailed description in **SI**). Overall, the latter suggested it is difficult to find a general design principle from these two kinds of observables (the structural change and solvation phenomenon in the active site).

In summary, through molecular understanding, we confirmed that in highly multiple ILs resistant variants M1a and M1b, the combination of surface charged and polar substitutions retained a higher number of essential water molecules in general. Hence, apart from the intrinsic stabilization, the increased hydration on the BSLA variant surface is highly important to maintain and improve BSLA ILs resistance and activity. This conclusion agrees well with the generally accepted concept that hydration is predominantly essential for proper enzyme dynamics to maintain enzyme structure and function [69, 112, 118].

3.6 A comprehensive view of IL-BSLA interaction and the potential application of design principles

IL with unusual characteristics holds the potential as a green media for many enzymatic reactions and protein preservation [68, 119, 120]. Even though the change in cation or anion, following by altering the polarity, hydrophobicity, viscosity of ILs, often influenced the catalytic reaction by disrupting

the structure, activity, stability, and enantioselectivity of the enzymes [68, 120]. A full understanding of these influences resulting from ILs can help researchers (re)engineer the enzyme for more efficient catalysis in ILs. By integration of the CompassR experimental recombination and the computational analysis, two complementary rational design principles to enhance ILs are proposed: (1) the advanced intrinsic stabilization (**section 3.4**); (2) strengthen hydration shells of the enzyme (**section 3.5**). Both design principles could be achieved in the protein engineering campaign by introducing the charged and/or polar residues into the enzyme surface with different gene mutagenesis techniques, such as SDM [39], reduced amino acid alphabets mutagenesis [55], and ordered synthetic gene.

Although the conformational/structural change of overall/local protein has a substantial impact on enzymes' stability and activity in ILs [69, 120], our results in **Figure S3-S5** suggest the structural observables are not the "best" candidates for proposing universal design principle. Besides, the different anions (e.g., halogen and TfO) presented various interaction phenomena (**Figure 5** and **Figure S6-S8**), supporting previous findings that the impact of the IL anion on the enzymes depends on its H-bond forming capability and nucleophilicity properties [68, 121]. Indeed, there is no single theory due to the complex nature of ion-enzyme interactions [68, 69, 114]. However, since these two summarized rational strategies do not involve the types of cations and anions in ILs, we thus believe that they can be applied for enzymes in most ILs and reduce the barrier to choosing or developing an IL to serve as solvent media.

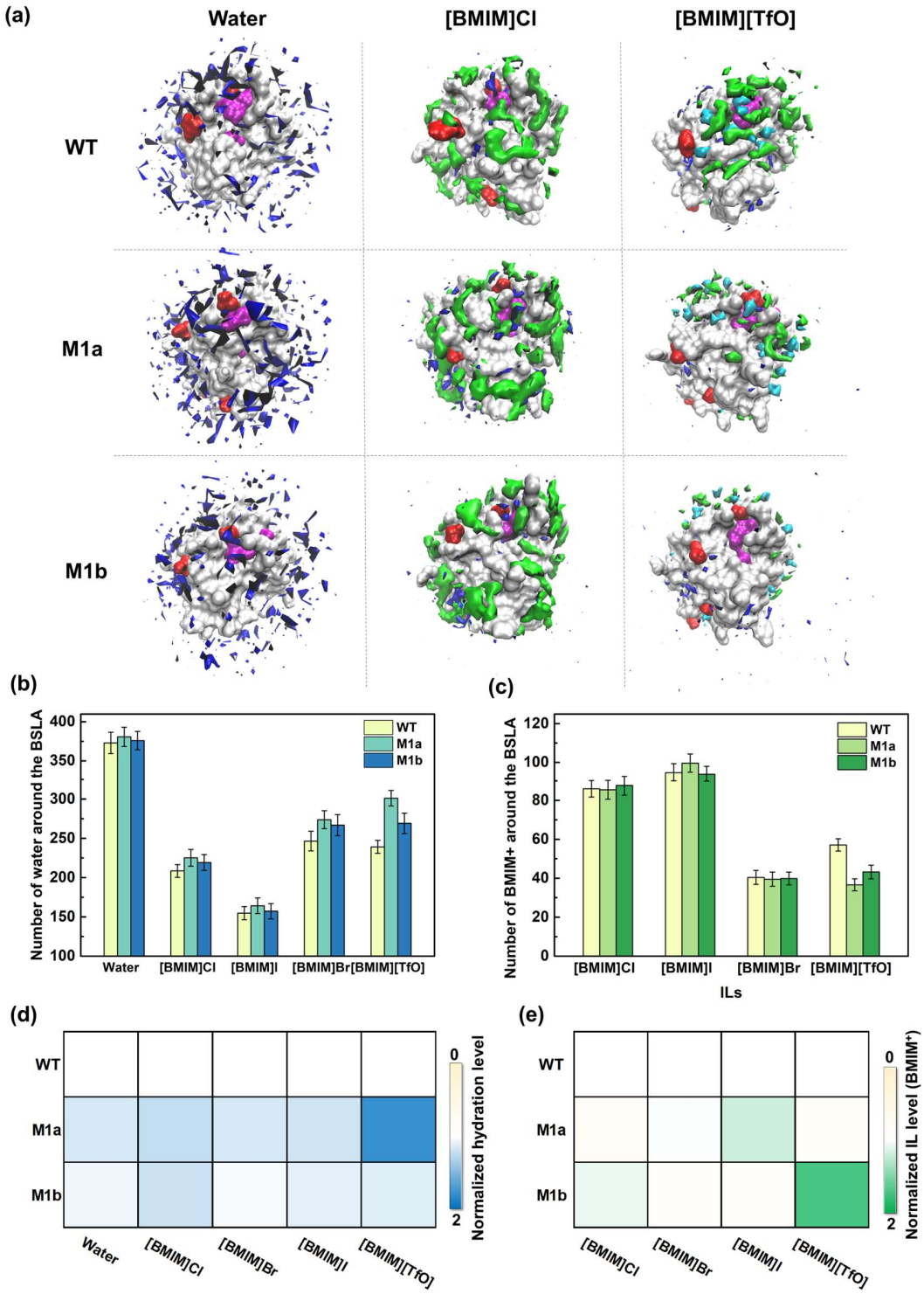

Figure 5. Solvation phenomenon around the WT and BSLA variants (M1a and M1b). (**a**) Spatial distribution of water and IL molecules at the molecular surface of the BSLA variant in water, [BMIM]Cl and [BMIM][TfO]. The BSLA surface is shown in grey, Ser77, Asp133, His156 (the catalytic triad) in magenta; the cation $BMIM^+$ molecules in green, anion molecules Cl^- , and TfO^-

in cyan; the water molecules in blue; and the substitutions in red. The 180° rotation of BSLA is shown in **Figure S6** to give a complete view of the surface. Each view of BSLA has the same orientation. The contours are shown with the isovalue 11 for water and isovalue 23, 37, 41 for $BMIM^+$, Cl^-, TfO^- molecules, respectively, in ILs systems. The contours are shown with the isovalue 110 for water in the pure water system. (**b**) The average number of water molecules interacting within the first solvation shell of the BSLA WT and variants. (**c**) The average number of $BMIM^+$ cations interacting within the first solvation shell of the BSLA WT and variants. (**d**) Hydration shell around the substituted sites relative to BSLA WT. (**e**) IL cation solvation level around the substituted sites relative to BSLA WT. Hydration level and IL solvation level averaged over the last 40 ns of MD trajectories. Water molecules whose O atom is within 3.5 Å distance cutoff of any non-hydrogen atom of BSLA were described as the first hydration shell and the number of water as hydration level [75]. A similar definition was also applied to the IL cation solvation level. The cutoff distance was determined from the radial distribution function (RDF) of $BMIM^+$ around BSLA residues when the "central" atom of IL cation molecule showed first minima approximately at this distance [75]. The "central" atom for $BMIM^+$ is N1. Consequently, a 6.5 Å cutoff was employed for $BMIM^+$ as our previous report [69].

Conclusion

CompassR analysis and computational-assisted selection of the positions (A81, G155, V165) enabled with minimal experimental efforts (~272 variants were generated) to significantly improve the BLSA resistance toward four ILs (up to 9-fold improvement in 18 % (v/v) [BMIM]Cl). The in-depth analysis demonstrated that the intrinsic protein stability and strengthened interaction between the hydration shells and the lipase are the main guiding principles for preserving lipase activity in ILs. Thereby CompassR enabled the identification of intrinsic stable BSLA variants with improved target properties, and MD simulations allowed efficient analysis of the stabilization of the hydration shell of BSLA. In addition, the gained molecular understanding generated an accurate and precise picture of BSLA-IL interaction. The combined computational approach (CompassR; analysis of hydration shell/lipase interactions) can likely serve as a blueprint to reengineer other enzymes for efficient catalysis in ILs (e.g., cellulases, hemicellulases, laccases for biomass degradation, and alcohol dehydrogenases for enantioselective reactions), thus further stimulating the broader application of biocatalysis in the emerging biobased economy. Since the

application of ILs as reaction media for biocatalysis can also bring out the substantial enhancement of selectivity, which yielding better product purities, easier downstream processing, and reduced waste, future studies should concentrate on estimating the performance of improved variants towards other substrates and/or reactions (e.g., acetylation, enantioselective reduction).

Supporting information (SI)

The Supporting Information is available free of charge on the Publications website at DOI:

ASSOCIATED CONTENT

AUTHOR INFORMATION

ORCID

Ulrich Schwaneberg: 0000-0003-4026-701X
Mehdi D. Davari: 0000-0003-0089-7156
Haiyang Cui: 0000-0001-8360-0447
Subrata Pramanik: 0000-0003-3328-6239
Karl Erich Jaeger: 0000-0002-6036-0708

Corresponding Author

Prof. Dr. Ulrich Schwaneberg

Dr. Mehdi D. Davari

Author contributions

Dr. H. Cui contributed to the ideas, investigation, data curation, formal analysis, and writing original draft and revision. Dr. S. Pramanik contributed to the molecular dynamics simulations. Prof. Dr. U. Schwaneberg and Dr. M. D. Davari contributed to the ideas, resources, supervision, writing and editing manuscript and revision. Prof. Dr. K. E. Jaeger contributed to the commentary and revision.

Conflict of Interest

The authors declare that they have no conflict of interest.

ACKNOWLEDGMENTS

Haiyang Cui is supported by a Ph.D. scholarship from the China Scholarship Council (CSC No. 201604910840). Simulations were performed with computing resources granted by JARA-HPC from RWTH Aachen University under projects JARA0169 and JARA0187.

References

1. P. Anastas and N. Eghbali, *Chem. Soc. Rev.*, 2010, **39**, 301-312.
2. P. T. Anastas and J. B. Zimmerman., *Environ. Sci. Technol.*, 2003, **37**, 94A-101A.
3. W. L. Hough, M. Smiglak, H. Rodríguez, R. P. Swatloski, S. K. Spear, D. T. Daly, J. Pernak, J. E. Grisel, R. D. Carliss and M. D. Soutullo, *New J. Chem.*, 2007, **31**, 1429-1436.
4. I. Marrucho, L. Branco and L. Rebelo, *Annu. Rev. Chem. Biomol. Eng.*, 2014, **5**, 527-546.
5. R. M. Moshikur, M. R. Chowdhury, M. Moniruzzaman and M. Goto, *Green Chem.*, 2020, **22**, 8116-8139.
6. A. G. Fadeev and M. M. Meagher, *Chem. Commun.*, 2001, 295-296.
7. A. P. Abbott, P. M. Cullis, M. J. Gibson, R. C. Harris and E. Raven, *Green Chem.*, 2007, **9**, 868-872.
8. J. Zhan, X. Zhang, R. Ma and Y. Tian, *Starch*, 2020, **72**, 1900120.
9. J. P. Mikkola, P. Virtanen, H. Karhu, T. Salmi and D. Y. Murzin, *Green Chem.*, 2006, **8**, 197-205.
10. R. A. Sheldon, R. M. Lau, M. J. Sorgedrager, F. van Rantwijk and K. R. Seddon, *Green Chem.*, 2002, **4**, 147-151.
11. N. L. Mai and Y.-M. Koo, in *Emerging Areas in Bioengineering*, 2018, pp. 35-65.
12. A. A. M. Elgharbawy, M. Moniruzzaman and M. Goto, *Biochem. Eng. J.*, 2020, **154**, 107426.
13. T. Itoh, *Chem. Rev.*, 2017, **117**, 10567-10607.
14. A. A. M. Elgharbawy, M. Moniruzzaman and M. Goto, *Curr. Opin. Green Sustain. Chem.*, 2021, **27**, 100406.
15. M. Reslan and V. Kayser, *Biophys. Rev.*, 2018, **10**, 781-793.
16. A. A. Elgharbawy, F. A. Riyadi, M. Z. Alam and M. Moniruzzaman, *J. Mol. Liq.*, 2018, **251**, 150-166.
17. M. Erbeldinger, A. J. Mesiano and A. J. Russell, *Biotechnol. Prog.*, 2000, **16**, 1129-1131.
18. C. Aouf, E. Durand, J. Lecomte, M.-C. Figueroa-Espinoza, E. Dubreucq, H. Fulcrand and P. Villeneuve, *Green Chem.*, 2014, **16**, 1740-1754.
19. M. K. Potdar, G. F. Kelso, L. Schwarz, C. Zhang and M. T. Hearn, *Molecules*, 2015, **20**, 16788-16816.
20. H. Liu, X. Wu, J. Sun and S. Chen, *Curr. Protein Pept. Sci.*, 2018, **19**, 100-111.
21. C. Hardacre and V. Parvulescu, *Catalysis in ionic liquirds: from catalyst synthesis to application*, Royal society of chemistry, 2014.
22. P. Xu, S. Liang, M.-H. Zong and W.-Y. Lou, *Biotechnol. Adv.*, 2021, 107702.
23. S. Slagman and W.-D. Fessner, *Chem. Soc. Rev.*, 2021.
24. R. A. Sheldon and J. M. Woodley, *Chem. Rev.*, 2018, **118**, 801-838.
25. H. Yamaguchi and M. Miyazaki, *Catal. Sci. Technol.*, 2021.
26. J. Ramos-Martín, O. Khiari, A. R. Alcántara and J. M. Sánchez-Montero, *Catalysts*, 2020, **10**, 1055.
27. X. Li, C. Zhang, S. Li, H. Huang and Y. Hu, *Ind. Eng. Chem.*, 2015, **54**, 8072-8079.
28. K. G. Sprenger, J. G. Plaks, J. L. Kaar and J. Pfaendtner, *Phys. Chem. Chem. Phys.*, 2017, **19**, 17426-17433.
29. R. Madeira Lau, F. Van Rantwijk, K. R. Seddon and R. A. Sheldon, *Org. Lett.*, 2000, **2**, 4189-4191.

30. J. Lai, Z. Hu, P. Wang and Z. Yang, *Fuel*, 2012, **95**, 329-333.
31. J. Zhao, N. Jia, K. E. Jaeger, M. Bocola and U. Schwaneberg, *Biotechnol. Bioeng.*, 2015, **112**, 1997-2004.
32. H. Liu, L. Zhu, M. Bocola, N. Chen, A. C. Spiess and U. Schwaneberg, *Green Chem.*, 2013, **15**, 1348-1355.
33. D. M. Mate and M. Alcalde, *Biotechnol. Adv.*, 2015, **33**, 25-40.
34. A. P. M. Tavares, O. Rodriguez and E. A. Macedo, *Biotechnol. Bioeng.*, 2008, **101**, 201-207.
35. J. Zhao, V. J. Frauenkron-Machedjou, A. Fulton, L. Zhu, M. D. Davari, K. E. Jaeger, U. Schwaneberg and M. Bocola, *Phys. Chem. Chem. Phys.*, 2018, **20**, 9600-9609.
36. E. M. Nordwald, G. S. Armstrong and J. L. Kaar, *ACS Catal.*, 2014, **4**, 4057-4064.
37. K. Nakashima, T. Maruyama, N. Kamiya and M. Goto, *Chem. Commun.*, 2005, 4297-4299.
38. E. M. Nordwald and J. L. Kaar, *J. Phys. Chem. B*, 2013, **117**, 8977-8986.
39. E. M. Nordwald and J. L. Kaar, *Biotechnol. Bioeng.*, 2013, **110**, 2352-2360.
40. H. Zhao, C. L. Jones and J. V. Cowins, *Green Chem.*, 2009, **11**, 1128-1138.
41. A. P. Tavares, O. Rodríguez, M. Fernández-Fernández, A. Domínguez, D. Moldes, M. A. Sanromán and E. A. Macedo, *Bioresour. Technol.*, 2013, **131**, 405-412.
42. X. Wu, F. Zhao, J. R. Varcoe, A. E. Thumser, C. Avignone-Rossa and R. C. Slade, *Bioelectrochemistry*, 2009, **77**, 64-68.
43. M. Persson and U. T. Bornscheuer, *J. Mol. Catal. B: Enzym.*, 2003, **22**, 21-27.
44. F. van Rantwijk, F. Secundo and R. A. Sheldon, *Green Chem.*, 2006, **8**, 282-286.
45. U. T. Bornscheuer, B. Hauer, K. E. Jaeger and U. Schwaneberg, *Angew. Chem., Int. Ed.*, 2019, **58**, 36-40.
46. L. Zhang, H. Cui, Z. Zou, T. M. Garakani, C. Novoa-Henriquez, B. Jooyeh and U. Schwaneberg, *Angew. Chem., Int. Ed.*, 2019, **58**, 4562-4565.
47. L. Zhang, H. Cui, G. V. Dhoke, Z. Zou, D. F. Sauer, M. D. Davari and U. Schwaneberg, *Chem. Eur. J*, 2020, **26**, 4974.
48. H. Yu, Y. Yan, C. Zhang and P. A. Dalby, *Sci. Rep.*, 2017, **7**, 41212.
49. H. Cui, L. Zhang, D. Söder, X. Tang, M. D. Davari and U. Schwaneberg, *ACS Catal.*, 2021, **11**, 2445-2453.
50. G. Qu, A. Li, C. G. Acevedo-Rocha, Z. Sun and M. T. Reetz, *Angew. Chem., Int. Ed.*, 2020, **59**, 13204-13231.
51. F. Cheng, L. Zhu and U. Schwaneberg, *Chem. Commun.*, 2015, **51**, 9760-9772.
52. D. Gonzalez-Perez, P. Molina-Espeja, E. Garcia-Ruiz and M. Alcalde, *PLoS One*, 2014, **9**, e90919.
53. R. J. Fox, S. C. Davis, E. C. Mundorff, L. M. Newman, V. Gavrilovic, S. K. Ma, L. M. Chung, C. Ching, S. Tam and S. Muley, *Nat. Biotechnol*, 2007, **25**, 338.
54. H. Cui, H. Cao, H. Cai, K. E. Jaeger, M. D. Davari and U. Schwaneberg, *Chem. Eur. J*, 2020, **26**, 643-649.
55. H. Cui, K.-E. Jaeger, M. D. Davari and U. Schwaneberg, *Chem. Eur. J*, 2021, **27**, 2789.
56. H. Cui, L. Zhang, L. Eltoukhy, Q. Jiang, S. K. Korkunç, K.-E. Jaeger, U. Schwaneberg and M. D. Davari, *ACS Catal.*, 2020, **10**, 14847-14856.
57. J. Xu, P. Xiong and B. He, *Bioresour. Technol.*, 2016, **200**, 961-970.
58. J. Pottkämper, P. Barthen, N. Ilmberger, U. Schwaneberg, A. Schenk, M. Schulte, N. Ignatiev and W. R. Streit, *Green Chem.*, 2009, **11**, 957-965.

59. J. L. L. Carter, M. Bekhouche, A. Noiriel, L. J. Blum and B. Doumèche, *Chembiochem*, 2014, **15**, 2710-2718.
60. M. Klähn, G. S. Lim and P. Wu, *Phys. Chem. Chem. Phys.*, 2011, **13**, 18647-18660.
61. T. De Diego, P. Lozano, S. Gmouh, M. Vaultier and J. L. Iborra, *Biomacromolecules*, 2005, **6**, 1457-1464.
62. R. M. Lau, M. J. Sorgedrager, G. Carrea, F. van Rantwijk, F. Secundo and R. A. Sheldon, *Green Chem.*, 2004, **6**, 483-487.
63. F. van Rantwijk, R. Madeira Lau and R. A. Sheldon, *Trends Biotechnol.*, 2003, **21**, 131-138.
64. V. J. Frauenkron-Machedjou, A. Fulton, L. Zhu, C. Anker, M. Bocola, K. E. Jaeger and U. Schwaneberg, *Chembiochem*, 2015, **16**, 937-945.
65. I. V. Pavlidis, D. Gournis, G. K. Papadopoulos and H. Stamatis, *J. Mol. Catal. B: Enzym.*, 2009, **60**, 50-56.
66. S. Ghaedizadeh, R. Emamzadeh, M. Nazari, S. M. M. Rasa, S. H. Zarkesh-Esfahani and M. Yousefi, *Biochem. Eng. J.*, 2016, **105**, 505-513.
67. D. Constantinescu, H. Weingärtner and C. Herrmann, *Angew. Chem., Int. Ed.*, 2007, **46**, 8887-8889.
68. M. Naushad, Z. A. Alothman, A. B. Khan and M. Ali, *Int. J. Biol. Macromol.*, 2012, **51**, 555-560.
69. S. Pramanik, G. V. Dhoke, K. E. Jaeger, U. Schwaneberg and M. D. Davari, *ACS Sustain. Chem. Eng.*, 2019.
70. H. Zhao, *J. Mol. Catal. B: Enzym.*, 2005, **37**, 16-25.
71. F. Stock, J. Hoffmann, J. Ranke, R. Störmann, B. Ondruschka and B. Jastorff, *Green Chem.*, 2004, **6**, 286-290.
72. P. R. Burney, E. M. Nordwald, K. Hickman, J. L. Kaar and J. Pfaendtner, *Recent Pat. Mater. Sci.*, 2015, **83**, 670-680.
73. A. Fulton, V. J. Frauenkron-Machedjou, P. Skoczinski, S. Wilhelm, L. L. Zhu, U. Schwaneberg and K. E. Jaeger, *Chembiochem*, 2015, **16**, 930-936.
74. S. A. Funke, N. Otte, T. Eggert, M. Bocola, K. E. Jaeger and W. Thiel, *Protein Eng., Des. Sel.*, 2005, **18**, 509-514.
75. H. Cui, T. H. Stadtmüller, Q. Jiang, K. E. Jaeger, U. Schwaneberg and M. D. Davari, *ChemCatChem*, 2020, **12**, 4073.
76. J. Schymkowitz, J. Borg, F. Stricher, R. Nys, F. Rousseau and L. Serrano, *Nucleic Acids Res.*, 2005, **33**, W382-W388.
77. J. Van Durme, J. Delgado, F. Stricher, L. Serrano, J. Schymkowitz and F. Rousseau, *Bioinformatics*, 2011, **27**, 1711-1712.
78. R. A. Studer, P. A. Christin, M. A. Williams and C. A. Orengo, *Proc. Natl. Acad. Sci. U. S. A.*, 2014, **111**, 2223-2228.
79. N. J. Christensen and K. P. Kepp, *J. Chem. Theory Comput.*, 2013, **9**, 3210-3223.
80. G. van Pouderoyen, T. Eggert, K. E. Jaeger and B. W. Dijkstra, *J. Mol. Biol.*, 2001, **309**, 215-226.
81. B. Hess, C. Kutzner, D. Van Der Spoel and E. Lindahl, *J. Chem. Theory Comput.*, 2008, **4**, 435-447.
82. S. Pall, M. Abraham, C. Kutzner, B. Hess and E. Lindahl, 2014.
83. E. Lindahl, B. Hess and D. Van Der Spoel, *J. Mol. Model*, 2001, **7**, 306-317.

84. D. Van Der Spoel, E. Lindahl, B. Hess, G. Groenhof, A. Mark and H. Berendsen, *J. Comput. Chem.*, 2005, **26**, 1701-1718.
85. N. M. Micaeˆlo and C. M. Soares, *J. Phys. Chem. B*, 2008, **112**, 2566-2572.
86. M. Kowsari, S. Alavi, M. Ashrafizaadeh and B. Najafi, *J. Chem. Phys.*, 2008, **129**, 224508.
87. M. Moreno, F. Castiglione, A. Mele, C. Pasqui and G. Raos, *J. Phys. Chem. B*, 2008, **112**, 7826-7836.
88. N. Schmid, A. P. Eichenberger, A. Choutko, S. Riniker, M. Winger, A. E. Mark and W. F. van Gunsteren, *Eur. Biophys. J.* , 2011, **40**, 843.
89. M. Rostkowski, M. H. Olsson, C. R. Søndergaard and J. H. Jensen, *BMC. Struct. Biol.* , 2011, **11**, 6.
90. T. J. Dolinsky, P. Czodrowski, H. Li, J. E. Nielsen, J. H. Jensen, G. Klebe and N. A. Baker, *Nucleic Acids Res.* , 2007, **35**, W522-W525.
91. K. E. Jaeger, B. W. Dijkstra and M. T. Reetz, *Annu. Rev. Microbiol.*, 1999, **53**, 315-351.
92. K. E. Jaeger and T. Eggert, *Curr. Opin. Biotechnol.*, 2002, **13**, 390-397.
93. L. Casas-Godoy, S. Duquesne, F. Bordes, G. Sandoval and A. Marty, *Methods Mol. Biol.*, 2012, **861**, 3-30.
94. P. Kusalik and I. Svishchev, *Science*, 1994, **265**, 1219-1221.
95. M. Fyta and R. Netz, *J. Chem. Phys.*, 2012, **136**, 124103-124111.
96. U. Essmann, L. Perera, M. L. Berkowitz, T. Darden, H. Lee and L. G. Pedersen, *J. Chem. Phys.*, 1995, **103**, 8577-8593.
97. J. Norberg and L. Nilsson, *Biophys J.*, 2000, **79**, 1537-1553.
98. A. Mor, G. Ziv and Y. Levy, *J. Comput. Chem.* , 2008, **29**, 1992-1998.
99. S. A. Pandit, D. Bostick and M. L. Berkowitz, *Biophys J.* , 2003, **84**, 3743-3750.
100. W. Humphrey, A. Dalke and K. Schulten, *J. Mol. Graph.*, 1996, **14**, 33-38.
101. M. T. Reetz, M. Bocola, J. D. Carballeira, D. Zha and A. Vogel, *Angew. Chem,. Int. Ed.*, 2005, **44**, 4192-4196.
102. J. C. Stevens, D. W. Rodgers, C. Dumon and J. Shi, *Front. Energy Res.*, 2020, **8**.
103. A.-M. Wallraf, H. Liu, L. Zhu, G. Khalfallah, C. Simons, H. Alibiglou, M. D. Davari and U. Schwaneberg, *Green Chem.*, 2018, **20**, 2801-2812.
104. I. Mateljak, A. Rice, K. Yang, T. Tron and M. Alcalde, *ACS Synth. Biol.*, 2019, **8**, 833-843.
105. Y. Ensari, G. V. Dhoke, M. D. Davari, A. J. Ruff and U. Schwaneberg, *Chembiochem*, 2018, **19**, 1563-1569.
106. Z. Sun, R. Lonsdale, X.-D. Kong, J.-H. Xu, J. Zhou and M. T. Reetz, *Angew. Chem., Int. Ed.*, 2015, **54**, 12410-12415.
107. N. Akbari, S. Daneshjoo, J. Akbari and K. Khajeh, *Appl. Biochem. Biotechnol.*, 2011, **165**, 785-794.
108. P. A. Muñoz, D. N. Correa-Llantén and J. M. Blamey, *Lipids*, 2015, **50**, 49-55.
109. P. A. M. Nascimento, F. P. Picheli, A. M. Lopes, J. F. B. Pereira and V. C. Santos-Ebinuma, *Biotechnol. Prog.*, 2019, **35**, e2838.
110. E. Firnberg, J. W. Labonte, J. J. Gray and M. Ostermeier, *Mol. Biol. Evol.*, 2014, **31**, 1581-1592.
111. C. J. Verbeek and L. E. Berg, *Recent Pat. Mater. Sci.*, 2009, **2**, 171-189.
112. D. Laage, T. Elsaesser and J. T. Hynes, *Chem. Rev.*, 2017, **117**, 10694-10725.

113. H. Cui, L. Eltoukhy, L. Zhang, U. Markel, K.-E. Jaeger, M. D. Davari and U. Schwaneberg, *Angew. Chem., Int. Ed.*, 2021, DOI: https://doi.org/10.1002/anie.202101642.
114. E. M. Nordwald, J. G. Plaks, J. R. Snell, M. C. Sousa and J. L. Kaar, *Chembiochem*, 2015, **16**, 2456-2459.
115. A. M. Figueiredo, J. Sardinha, G. R. Moore and E. J. Cabrita, *Phys. Chem. Chem. Phys.*, 2013, **15**, 19632-19643.
116. H. S. Kim, S. H. Ha, L. Sethaphong, Y. M. Koo and Y. G. Yingling, *Phys. Chem. Chem. Phys.*, 2014, **16**, 2944-2953.
117. H. S. Kim, D. Eom, Y. M. Koo and Y. G. Yingling, *Phys. Chem. Chem. Phys.*, 2016, **18**, 22062-22069.
118. J. N. Dahanayake and K. R. Mitchell-Koch, *Front. Mol. Biosci.*, 2018, **5**, 65.
119. J. C. Stevens, L. Das, J. K. Mobley, S. O. Asare, B. C. Lynn, D. W. Rodgers and J. Shi, *ACS Sustain. Chem. Eng.*, 2019, **7**, 15928-15938.
120. L. Bui-Le, C. J. Clarke, A. Bröhl, A. P. S. Brogan, J. A. J. Arpino, K. M. Polizzi and J. P. Hallett, *Commun. Chem*, 2020, **3**, 55.
121. H. Zhao, G. A. Baker, Z. Song, O. Olubajo, L. Zanders and S. M. Campbell, *J. Mol. Catal. B Enzym.*, 2009, **57**, 149-157.

1